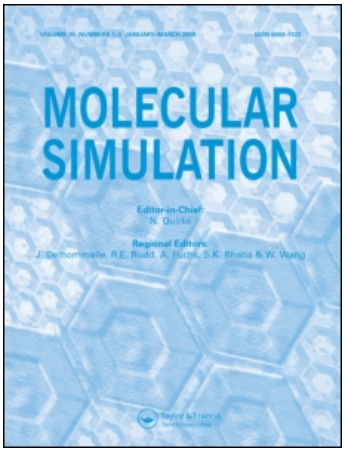

Molecular Simulation
Publication details, including instructions for authors and subscription information:
http://www.informaworld.com/smpp/title~content=t713644482

Molecular Dynamics Simulations of Proton Transfer in a Model Nafion Pore

E. Spohr[a]
[a] Institut für Werkstoffe und Verfahren der Energietechnik (IWV-3) Forschungszentrum Jülich, Jülich, Germany

To cite this Article Spohr, E.(2004) 'Molecular Dynamics Simulations of Proton Transfer in a Model Nafion Pore', Molecular Simulation, 30: 2, 107 — 115
To link to this Article: DOI: 10.1080/0892702301000152208
URL: http://dx.doi.org/10.1080/0892702301000152208

Molecular Simulation, VOL. 30 (2–3), 15 February–15 March 2004, pp. 107–115

Molecular Dynamics Simulations of Proton Transfer in a Model Nafion Pore

E. SPOHR*

Institut für Werkstoffe und Verfahren der Energietechnik (IWV-3) Forschungszentrum Jülich, D-52425 Jülich, Germany

(Received October 2002; In final form December 2002)

Proton conducting polymer electrolyte membranes (PEM) for fuel cell applications often contain a sulfonated perfluorinated side chain, which is attached to a polymeric backbone. Proton conductance in such membranes is a complicated process, which depends on both material properties and operational parameters of the fuel cell. Experimentally, it is well established that proton conductivity in such membranes is strongly dependent on water content, approaching that of bulk water at high water content. The goal of the present study is to analyze the relationship between pore structure on the molecular level and proton transfer dynamics as a function of water content and side chain density. A molecular model of the side chain has been developed and is used to simulate proton transport in a simple slab pore. The polymer backbone is represented as a simple excluded volume, described by a Lennard–Jones interaction potential.

Keywords: Proton transfer; Model Nafion Pore; Polymer electrolyte membrane; Direct methanol fuel cell

INTRODUCTION

The polymer electrolyte membrane (PEM) is a key component of both the hydrogen (PEFC) and direct methanol fuel cell (DMFC) [1,2]. It provides the transport medium for the protons generated during the anodic oxidation reaction of the fuel. The demands on the PEM by a working low temperature fuel cell are (i) high proton conductivity (ii) low permeation of water and fuel and (iii) long-term mechanical and thermal stability as well as stability in acidic environments. Fulfilling all these demands at the same time provides a major challenge to material science in fuel cell research. Currently, the most widely used membrane materials consist of a perfluorinated polymer backbone with perfluorinated oligo-ether side chains [3–5]. The side chains are terminated by strongly acidic sulfonic acid head groups. When exposed to water or humid air, the membrane takes up large amounts of water (more than 20 water molecules per sulfonic acid group), and it swells, leading to a bicontinuous nano-phase separated network of aqueous pores and polymer. At the same time, the sulfonic acid groups dissociate and the material becomes proton-conducting. The conductivity increases with increasing water content and depends on the density of sulfonate groups [1]. From the temperature dependence of the proton conductivity in dry and wet membranes [6,7], it has been concluded that protons appear to be transported by hopping from one sulfonate group to the next in dry membranes, and that the proton transport mechanism in wet membranes becomes similar to that in bulk acid solutions (see below).

In investigating proton transport in PEMs on the molecular level, one has to tackle two problems: (i) The membrane is dynamic. Shape and size of individual pores and the connectivity of the pore network change with time. An adequate description of these processes requires very long simulation times. (ii) Both Experimental [6,7] and theoretical [8–10] evidence indicate that at high water content, which is typical for fuel cell applications, structural diffusion of protons, the so-called Grotthus mechanism [11], becomes important. In this non-classical transport mechanism, one proton of a hydronium ion, H_3O^+, is transferred to a neighboring water molecule. An intermediate adduct similar to the so-called

*E-mail: e.spohr@fz-juelich.de

ISSN 0892-7022 print/ISSN 1029-0435 online © 2004 Taylor & Francis Ltd
DOI: 10.1080/0892702301000152208

Zundel complex $H_5O_2^+$ is formed which can then dissociate into a water molecule and a hydronium ion. The essential correctness of this mechanism has been supported by recent Car-Parrinello molecular dynamics (MD) simulations [12]. Such simulations, however, cannot be carried out with present-day computers for the complex membrane/water system present in a wet PEM.

To date, simulations focused on one of the two issues. Water/PEM interfaces were studied by classical MD, focusing on the dynamics of simple ions such as Na^+ or K^+ in water/Nafion [13], methanol/Nafion [14], or water/methanol/Nafion mixtures [15], or spherical hydronium models (a "large" ion) in PEMs [16]. Non-classical Grotthus transport of protons in PEMs was not investigated. In these studies, the polymer phase consists of rather short chains. Although polymer dynamics is included to some extent, it can not be expected that the simulations cover much of the relevant polymer dynamics, due to rather short simulation times on the time scale of about 1 ns. Paddison *et al.* studied Nafion fragments such as CF_3SO_3H and the pendant Nafion side chain [17–20] with molecular modeling techniques but did not perform long dynamic simulations that yield transport coefficients.

Proton dynamics in bulk water, on the other hand, was investigated using classical hydronium models (e.g. Refs. [21,22]), mixed quantum/classical dynamics [23,24], *ab initio* and Car-Parrinello "ab initio" MD technique [12,25–30] and by using so-called empirical valence bond (EVB) models [31–38]. The latter class of models provides an interesting compromise between physical adequacy and computational effectiveness and thus allows the study of non-classical proton transport on a much longer time scale than "ab initio" MD, and for a much more complex system. However, by construction, most multi-state EVB models are unsuitable for highly concentrated proton solutions as they occur in a PEM. Walbran and Kornyshev [39] developed a simple local polarizable two-state EVB model which overcomes this difficulty, however, at the expense of a somewhat too high water diffusion coefficient and a somewhat too low proton conductivity. It does, however, implement the Grotthus mechanism of proton transport in a very efficient way.

One goal of the research done in our institute is to understand the mechanisms of proton transfer in PEMs and to calculate proton mobility for membranes with different chemical and/or physical characteristics. In a recent study on proton transport in polymer membranes [40] we combined for the first time in MD simulations non-classical proton dynamics with an (admittedly simple) polymer environment. In that study, the polymer backbone was approximated by an excluded volume. No attempt was made to study the entire pore network. Instead, simulations of single slab pores were performed. Various simple models describing the sulfonate group, the side chain and its motional degrees of freedom were simulated, in order to elucidate the most important environmental influences on proton dynamics. The property of the PEM phase which influences proton dynamics the most was found to be the nature of the charge distribution on the sulfonate group, followed by SO_3^- head group dynamics. In that study, the importance of modeling the Nafion side chain was also investigated. In the present study, we analyze the side chain model in more detail and study the interplay between structure and dynamics of this realistic PEM pore, modeled as a slab confined by Nafion side chains, as a function of water content and side chain density.

SIMULATION MODELS AND METHODS

Molecular simulation of transport in PEMs requires the inclusion of two features in the models, which are hard to fulfill simultaneously: (i) The model must be simple enough to allow for long simulation times, since very slow motions of the polymer chains may ultimately be responsible for the experimentally observed conductivity. (ii) On the other hand, the model must be able to describe the complex, non-classical transport of protons in aqueous environments, as it is born out by the proposed Grotthus mechanism [11], which was recently, by and large, verified for the bulk phase of water by Car-Parrinello type simulations [12].

Here we focus on the proton transfer dynamics and neglect the large scale polymer dynamics by simulating only a single pore between rigid backbone walls. In an EVB model, the adiabatic ground state of a proton is described through a superposition of two or more diabatic basis states, each of which represents a specific arrangement of chemical bonds in which the excess proton is bound to a specific water molecule (classical VB states). These states are coupled by off-diagonal elements and diagonalization of the (classical) Hamiltonian matrix leads to the proton ground state. The basic unit of the polarizable two-state EVB model used here [39] is the Zundel complex $H_5O_2^+$. The model consists of two basis states which correspond to the (equivalent) complexes $H_3O^+ \cdot H_2O$ and $H_2O \cdot H_3O^+$. At any given time, there is one "active" hydrogen atom, named H_B which can be transferred and which is the central proton in the Zundel complex as displayed in Fig. 1. The proton transfer coordinate $q := r_1 - r_2 (\leq 0)$ characterizes the internal state of the Zundel complex: $q \approx 0$ refers to symmetrical Zundel ions, $q \leq -0.5$ Å refers to the situation when the Zundel ion (temporarily) decomposes into a hydronium ion,

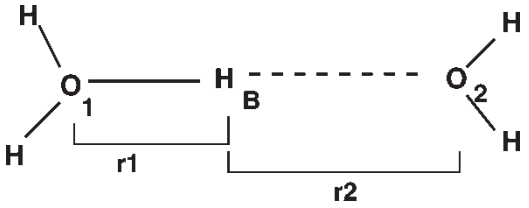

FIGURE 1 Schematic drawing of the basic EVB (Zundel) $H_5O_2^+$ complex.

H_3O^+, and a water molecule. The local nature of the coupling between the two basis states and an empirical charge switching function makes the simulation of systems with high proton concentrations possible, since only two water molecules contribute to each adiabatic state. Further details can be found in Refs. [39,40].

In the current study, water and proton-filled slab-like pores of fixed width are investigated. Figure 2 shows a snapshot of such a system. In a typical simulation, several hundred or thousand water molecules and 40–80 protons are confined into a slab of 25 Å width. The confinement is realized via an oxygen-wall potential of 12-6 LJ type

$$V_{\text{O-wall}} = 4\varepsilon\left[\left(\frac{\sigma}{z-z_0}\right)^{12} - \left(\frac{\sigma}{z-z_0}\right)^{6}\right] \qquad (1)$$

with $\varepsilon = 95.94 \times 10^{-23}$ J, $\sigma = 3.223$ Å and $z_0 = \pm 12.5$ Å. This corresponds to a well depth of 0.2 kT at $T = 298.15$ K (with Boltzmann's constant k and the temperature T). Hydrogen atoms do not interact with the wall. The precise form of the wall potential is of little importance, since its well depth is rather shallow and its primary purpose is to produce the excluded volume due to the polymer backbones.

This wall potential, serving as a crude model for the main chain, is augmented by a molecular description of the side chains. The end atoms of the side chain, i.e. the ether oxygen atoms which connect to the main chain are constrained to move only on a plane which is set to 1 Å beyond the wall (which is located at ±11.5 Å). With the exception of this single constraint, the side chains are completely flexible. Specifically, they can undergo conformational changes. The interaction parameters for the side chains are based on the Dreiding force field [41] and are chosen to agree largely with the Nafion model of Vishnyakov and Neimark [15]. The standard Lorentz–Berthelot combination rules have been applied for Lennard–Jones interactions. This force field is a combination of intermolecular electrostatic and (12-6) Lennard–Jones terms and intra-molecular stretch, bend and torsional degrees of freedom. The parameters are collected in Table I. For reasons discussed in Ref. [40], the partial charges have been chosen differently from the original work in Ref. [15]. These changes relate to the distribution of the negative counter charge between sulfonate group and the rest of the side chain. In the model used here, the SO_3^- group carries the full negative charge; ether oxygen atoms and CF_2 groups are electro-neutral entities.

We have simulated three systems (A,B,C) at rather high water content λ, with λ the ratio of water molecules, n_w, to protons n^+. Between 14 and 39 water molecules per proton were used,

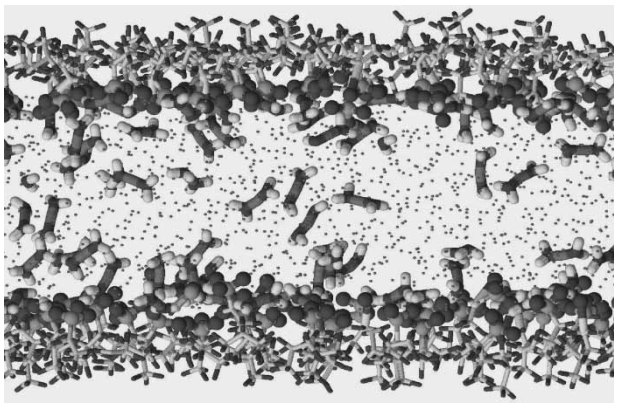

FIGURE 2 Snapshot of the simulation box of run B. The side chains and Zundel complexes are depicted using ball-and-stick representations. Only oxygen atoms of non-Zundel water molecules are shown as small dots.

TABLE I Force field parameters

Lenard–Jones parameters and partial charges q $V = 4\varepsilon\left[\left(\frac{\sigma}{r}\right)^{12} - \left(\frac{\sigma}{r}\right)^{6}\right]$			
	ε/kJ mol^{-1}	σ/Å	q/e
C	0.3981	3.473	0.450
F	0.3035	3.093	− 0.225
O_e	0.7117	3.070	0.000
S	1.0465	3.550	1.190
O_s	0.8372	3.150	− 0.730
Stretch parameters: $V = \frac{1}{2}k(r - r_0)^2$			
	k/kJ mol^{-1} Å^{-2}	r_0/Å	
C—C	2928.8	1.54	
C—O_e	2928.8	1.54	
C—F	2928.8	1.37	
C—S	2928.8	1.80	
S—O_s	2928.8	1.49	
Bend parameters: $V = \frac{1}{2}k_\alpha(\cos\alpha - \cos\alpha_0)^2$			
	k_α/kJ mol^{-1} rad^{-2}	α_0	
C—C—C	471.45	109.60°	
C—C—F	472.04	109.70°	
F—C—F	470.70	109.47°	
S—C—C	490.91	112.60°	
S—C—F	478.15	110.70°	
O_s—S—C	456.31	106.75°	
O_s—S—O_s	509.36	115.00°	
O_e—C—C	470.70	109.47°	
C—O_e—C	470.70	109.47°	
O_e—C—F	470.70	109.47°	
All torsion terms: $V = \frac{1}{2}k_\phi[1 - \cos[3 \times (\phi - \pi)]], k_\phi = 0.9297$ kJ mol^{-1}			

TABLE II Simulation parameters

Run	n_o	n^+	λ	A	D_σ	$\langle r_{O_e} - S\rangle$	$\bar{\tau}_{HH}$	$\bar{\tau}_{ZZ}$	t_{sim}
A	560	40	14	43.4	1.9 ± 0.2	5.48	3.8	7.6	400
B	1528	80	19	61.9	3.2 ± 0.2	5.78	3.4	7.2	250
C	1528	40	38	123.8	4.6 ± 0.2	5.82	3.4	7.0	350

n_o and n^+ are the number of oxygen atoms and the number of protons, respectively. $\lambda = n_o/n^+$ is the water content, A (in Å^2) the area per SO_3^- group. D_σ is the proton diffusion coefficient, calculated via $D_\sigma = \lim_{t\to\infty}\langle[x(t) - x(0)]^2 + [y(t) - y(0)]^2\rangle/4t$ from the mean square displacement in the two directions parallel to the pore surface (in units of 10^{-5} cm^2 s^{-1}) $\langle r_{O_e} - S\rangle$ (in Å) is the mean end-to-end distance of the side chain (the distance between the S atom of the sulfonate group and the terminal ether oxygen O_e). $\bar{\tau}_{HH}$ and $\bar{\tau}_{ZZ}$ are the mean hopping times (in ps) between two H_3O^+ ions and two $H_5O_2^+$ ions, respectively (see text). t_{sim} is the total simulation time (in ps).

which corresponds to proton concentrations approximately between 1.3 and 4 mol l^{-1}. The systems differ by the mean area A per side chain or, equivalently, the interfacial charge density produced by the SO_3^- groups, the number of which is equal to the number of protons, thus rendering the system electro-neutral. Varying the area A is in some ways equivalent to simulating materials with different equivalent weight, i.e. a different chain volume per SO_3^- group. At the same time, the water content λ varies over the three simulations. After extensive equilibration periods between 50 and 150 ps, all simulations were run at 298.15 K over the simulation time specified in Table II, using the velocity version of the Verlet algorithm with a time step length of 0.25 fs. The Berendsen thermostat [42] was used with a time constant of 1 ps to maintain the average temperature.

RESULTS

Density Profiles

Density profiles $\rho(z)$ along the z direction perpendicular to the pore interface have been calculated. Figure 3 shows these profiles for all oxygen atoms (water oxygen and oxygen atoms of Zundel complex) as long dashes, the transferring protons H_B as full lines and the S atoms of the SO_3^- groups as short dashes for the three different water contents. The first, expected, observation is that the oxygen distribution does not depend strongly on the density of sulfonate groups on the surface. For all levels of water content investigated, protons are found throughout the slab. This can also be inferred from the snapshot in Fig. 2. With increasing proton concentrations, more and more protons are pushed towards the surfaces of the slab, while the proton concentration in the center increases only slightly. In all cases, the proton and the sulfonate S distributions overlap significantly. At the lowest water content, $\lambda = 14$, the distribution of sulfur atom is wider than in the other cases. At the same time, the mean end-to-end distance of the side chain is shorter (see Table II). Hence, the side chain is more compact at lower water content.

Pair Correlation Functions

Since only the z position of the terminal ether oxygen atom is constrained, the Nafion side chains are free to arrange themselves laterally. Figure 4 shows the sulfur–sulfur pair correlation functions for all three simulations. The mean nearest neighbor distance between two sulfur atoms increases from around 6 Å to about 7 Å with decreasing side chain density or increasing λ.

Figure 5 shows two-dimensional pair correlation functions between sulfonate S atoms and transferring protons H_B (see Fig. 1) as a function of the distance component $\rho = (x^2 + y^2)^{1/2}$ parallel and the distance component z perpendicular to the surface plane. The nearest neighbor maximum is located around $(\rho, z) \approx (4.5, 1.5)$, which means that a Zundel ion is part of the solvation shell of the sulfonate group. At the higher proton and SO_3^- concentration (bottom) the slope of the maximum ranges further into the region $z < 0$, which indicates that the protons are partially located *in the plane* of the sulfonate head groups. The density profiles in Fig. 3 support this view, as the sulfonate density distribution is substantially wider for $\lambda = 14$. With increasing λ, a second neighbor maximum in the pair correlation function is located around $(\rho, z) \approx (7, 1)$.

In all simulations a semicircular ring of high S—H_B correlation is observed. This feature implies that there is a hemispherical region around each S atom over which the protons are distributed. The almost constant height of this ridge implies that there is no large barrier for the motion of the proton within the solvation shell of a sulfonate ion. The ridge, together with the maximum located around $(\rho, z) \approx (4.5, 1.5)$, thus characterizes the distribution of a proton within the solvation shell of one sulfonate ion, where the most probable situation is the one where the Zundel complex is located sideways between sulfonate groups, forming hydrogen bonds to the SO_3^- oxygen atoms.

The second maximum located around $(\rho, z) \approx (7, 1)$ reflects the correlation of the proton with a second neighbor SO_3^- group. Its height relative to the first maximum is the more pronounced, the larger the water content λ.

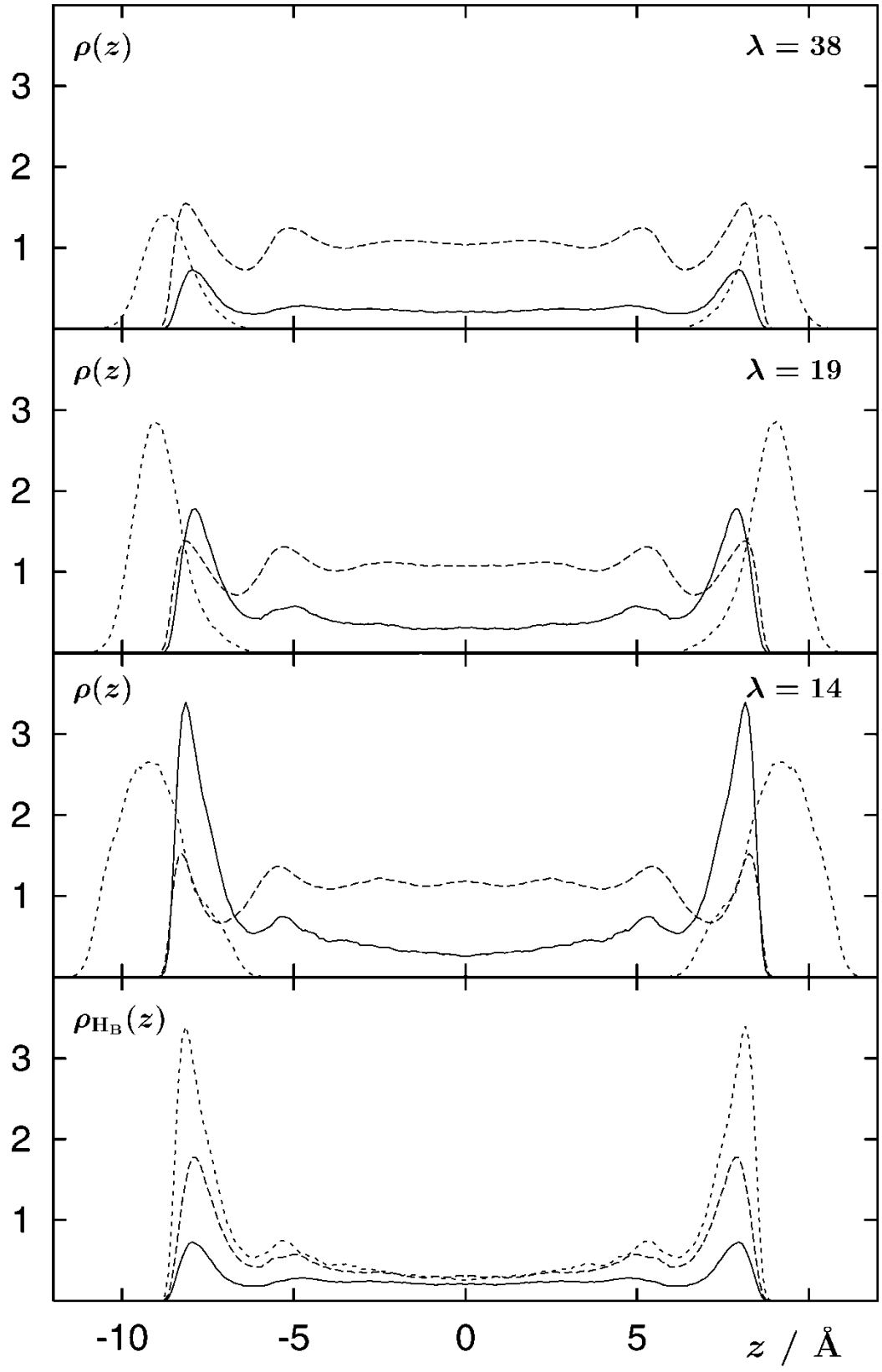

FIGURE 3 Atom density profiles. The top three frames contain the active proton (H_B) profiles (full line), the oxygen atom profiles (oxygen atoms of water molecules and of Zundel complexes; long dashes) and the SO_3^- sulfur atom profiles (short dashes) for the three simulations with different water contents as indicated. The bottom frame contains the three hydrogen profiles also depicted above. For better visibility, the H_B and S profiles are scaled by a factor of 10.

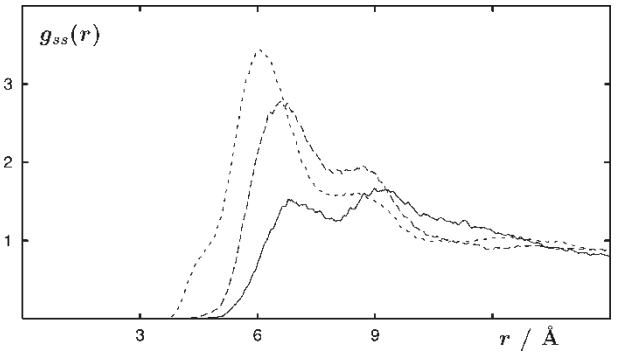

FIGURE 4 Sulfur–sulfur pair correlation functions for $\lambda = 38$ (full line), 19 (long dashes) and 14 (short dashes).

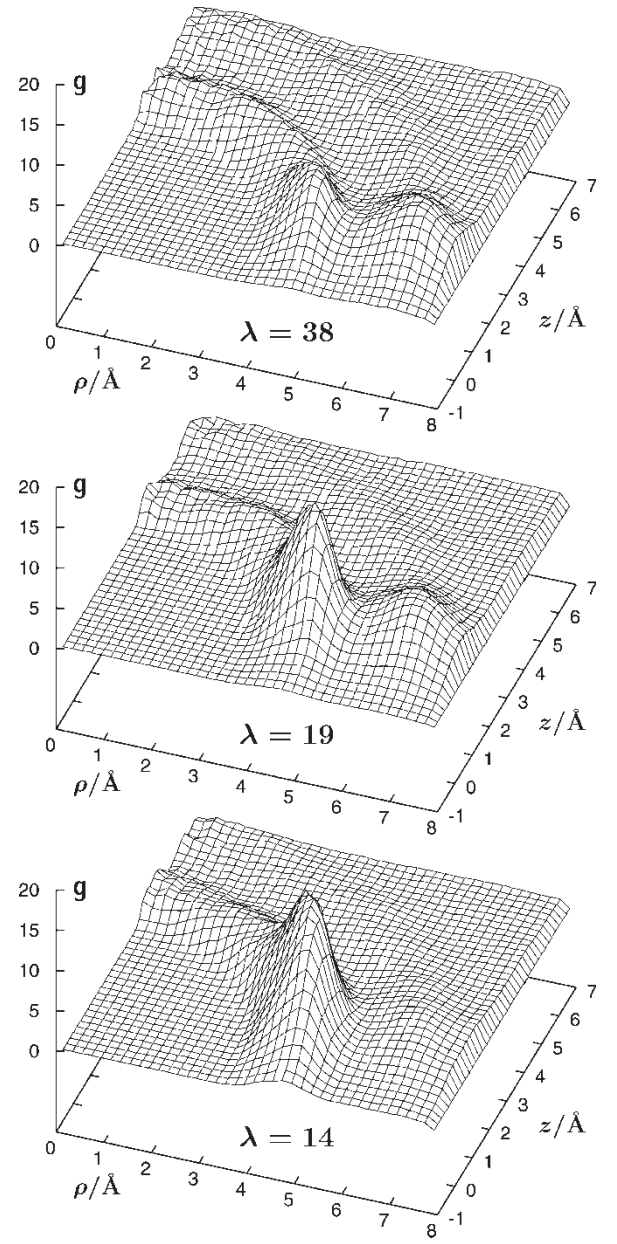

FIGURE 5 Two-dimensional sulfur–proton pair correlation functions $g_{S\text{-}H_B}(\rho,z)$. ρ is the distance component parallel to the interfacial plane, z the component perpendicular to the surface. Water content λ as given in the plot.

Proton Dynamics

Table II contains data about the proton transfer dynamics. The focus is on the single particle dynamics and thus on proton self diffusion coefficients, since they can be calculated more reliably than the conductivity, which describes the collective dynamics of all the protons in the pore. The diffusion coefficient D_σ of the proton defect is calculated from the final slope of the mean square displacement of the H_B atom over a period of 25 ps. Clearly, proton mobility as characterized by D_σ increases with increasing water content. This agrees well with the experimental evidence in Nafion and similar membranes [1,6,7]. The bottom frame of Fig. 3 shows that with increasing proton concentration (increasing sulfonate density and decreasing water content), an increasing *fraction* of the protons are *adsorbed* near the surface layer formed by the sulfonate ions. This behavior has two origins: first, with increasing proton concentration in the bulk, ionic repulsion will increase and push the ions towards the interfaces. This would be the case even if there were no SO_3^- head groups present. Second, the increasing surface charge density with increasing SO_3^- concentration increases the electrostatic adsorption energy. In total, the observed effect is consistent with Gouy-Chapman theory, since with increasing concentration of free ions the double layer thickness should decrease. If one assumes that the Nernst relationship holds approximately, i.e. one assumes that the conductivity $\Lambda \propto D \times c$ with c, the total proton concentration, one would expect rather similar values for the proton conductivity. Thus, the proton conductivity in membranes approaches an approximately constant value at high water content due to the balance between the decreasing proton concentration on the one hand and the increasing mobility of the individual proton on the other hand.

The EVB model describes proton transport as a sequence of interconversions between Zundel and H_3O^+ complexes [39]. Thus, non-classical proton transfer occurs through a series of $H_5O_2^+ \rightarrow H_3O^+$ and subsequent $H_3O^+ \rightarrow H_5O_2^+$ steps. These interconversions are rapid and fluctuating in nature. Conversions $H_5O_2^+ \rightarrow H_5O_2^+$ or $H_3O^+ \rightarrow H_3O^+$ are significantly slower and more likely to be rate-determining. However, it was found for the present model [43] that such conversions between nearest neighbor oxygens have a high probability to be anti-correlated, i.e. that the second $H_3O^+ \rightarrow H_3O^+$ conversion leads, with a high probability, to the original H_3O^+ ion. The same holds for $H_5O_2^+ \rightarrow H_5O_2^+$ conversions, in which one oxygen atom is shared by the initial and final complexes. Thus, these processes are not "reactive", i.e. they do not lead to proton transport. On the other hand, $H_3O^+ \rightarrow H_3O^+$

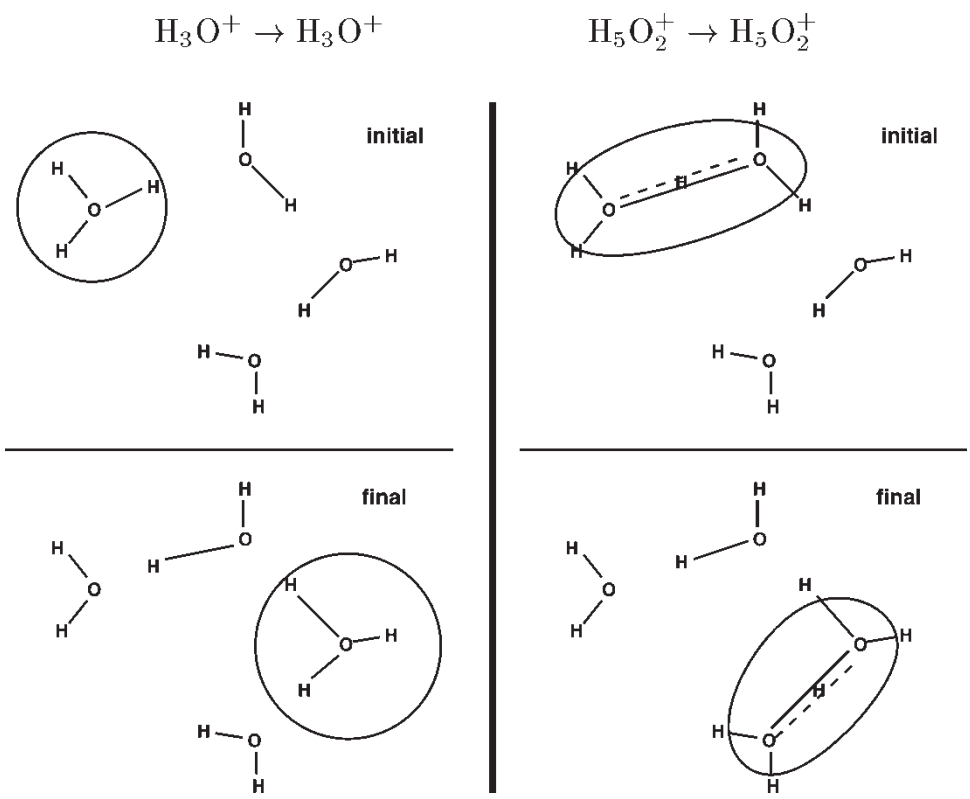

FIGURE 6 Sketches of proton transfer scenarios. Left: proton transfer from an initial H_3O^+ state to a second-neighbour final H_3O^+ state. The characteristic time for such a transfer is $\bar{\tau}_{HH}$. Right: proton transfer from an initial $H_5O_2^+$ state to a neighbouring final $H_5O_2^+$ state. The characteristic time for such a transfer is $\bar{\tau}_{ZZ}$.

jumps to second nearest neighbors and $H_5O_2^+ \rightarrow H_5O_2^+$ jumps, in which the initial and final Zundel complex do not share any oxygen atoms, appear to be a better measure for the characteristic proton hopping time [43]. Sketches of the initial and final states for these jumps are shown in Fig. 6.

Table II contains such hopping times $\bar{\tau}_{HH}$ for $H_3O^+ \rightarrow H_3O^+$ and τ_{ZZ} for $H_5O_2^+ \rightarrow H_5O_2^+$ transformations. The time of formation of a particular H_3O^+ ion is defined as the first time when the proton transfer coordinate q becomes smaller than -0.45 Å with a particular oxygen at the center of the complex. Then the time τ is measured, until another H_3O^+ ion is formed for the first time, where the oxygen atom is not a nearest neighbor of the original H_3O^+ ion. Analogously, the time of formation of a particular $H_5O_2^+$ ion is defined as the first time, when q becomes larger than -0.05 Å. Then, the time τ is measured, until for the first time another $H_5O_2^+$ ion is formed, which does not contain any of the original two oxygen ions. The table contains the averages calculated according to $\bar{\tau} = \langle \tau^{-1} \rangle^{-1}$.

One observes that the mean hopping time between two $H_5O_2^+$ ions is about twice as long as that between two H_3O^+ ions. Indeed the symmetric $H_5O_2^+$ ion state is found to have a higher weight than the asymmetric $H_3O^+ \cdot H_2O$ state (not shown). In this respect, the two-state EVB model differs from the more sophisticated density functional simulation results [12]. Interestingly, the hopping times do not change much with water content.

DISCUSSION

Experimental data for perfluorinated PEMs such as Nafion (DuPont), Dow (Dow Chemicals) and others show that the proton conductivity increases both with increasing water content and with decreasing equivalent weight of the polymer, i.e. with decreasing polymer volume per SO_3^- head group. At high water content, however, the conductivity reaches a plateau value. Depending on material, the plateau value of good membranes is slightly different and is reached more or less rapidly with increasing water content [1]. The shape and size distribution of aqueous pores in such wet membranes is not very well known and depends to some extent on the processing history. Typical compartment sizes in the nano-phase-separated materials are of the order of 2–5 nm, depending on material and experiment [44–49].

In the present study, three single slab pores were simulated, which serve as models of characteristic pores occurring in the most widely used fuel cell membrane material Nafion. The polymer backbone is represented by an excluded volume for the aqueous

phase, which consists of water and protons. Nafion side chains $O{-}CF_2{-}C(F,CF_3){-}\ O{-}CF_2{-}CF_2{-}SO_3^-$ are modeled with full molecular detail. The three pores studied here have a constant thickness and differ by the number of side chains per unit area and thus by the number of protons in the slab. Varying the side chain area or, equivalently, the charge density models to some extent, materials with different equivalent weight, i.e. a different chain volume per SO_3^- group. At the same time, the ratio λ of water molecules to protons is varied as well, which corresponds to changing one of the operating conditions of a fuel cell, namely the humidity.

The proton diffusion coefficient (as characterized by the motion of the H_B defects in the solution) is found to increase with increasing water content λ or, equivalently, with decreasing surface charge density (increasing area) of the polymer phase. The increase in diffusion coefficient is accompanied by a more homogeneous distribution of protons within the pore. With increasing surface charge density (and proton concentration), there is increased ion pair formation between $H_5O_2^+$ complexes and SO_3^- head groups. In interfacial electrochemistry, one would call it proton "adsorption" at the interface (see Fig. 3). Thus, the double layer thickness decreases with increasing proton concentration, as expected on the basis of Gouy–Chapman and more elaborate theories. This means, since there is no background electrolyte present in the pore, that with increasing concentration more and more protons become strongly immobilized due to the ion pair formation. This explains the observed decrease in diffusion coefficient with decreasing λ.

Since the total conductivity of the membrane is, assuming the validity of the Nernst relation, approximately proportional to the product of proton concentration and diffusion coefficient, the two effects balance each other. For the three simulations performed here, this would mean that a similar plateau value for the conductivity is reached at different water content. Since high proton conductivity at low water content is desirable for operation of fuel cells, this favors the low equivalent weight materials.

Some information on the mechanism of proton transport in such membrane pores can be derived from the simulation. Two basic possibilities exist: First, it is conceivable that proton transport predominantly occurs through the center of the pore (bulk mechanism). Second, transport can occur by proton hopping along the SO_3^- groups ("adsorption sites") along the water/polymer interface (surface mechanism). A more detailed discussion can be found in Ref. [8–10,40]. Here, the pair correlation functions in Fig. 5 and the density profiles in Fig. 3 indicate that proton motion proceeds indeed in the vicinity of the SO_3^- species. On the other hand, the rather short proton hopping times $\bar{\tau}$ in Table II, which are independent of water content, are similar to the corresponding times found in bulk water [43], which in turn points towards an important contribution of the Grotthus mechanism to the proton transport in PEM pores. From studies at a single temperature no definitive conclusions about the rate-determining step can be drawn. In order to clarify this point, we currently investigate the temperature dependence of proton transport in membrane pores of varying thickness, using a simpler model of the polymer phase, where only SO_3^- head groups are explicitly modeled [50]. It can be expected that with decreasing pore size, the activation energy of proton transport should increase when the surface hopping mechanism becomes rate determining at low water content.

Finally, it should be noted that the model pore system discussed here is artificial and requires several *ad hoc* assumptions. For instance, the pore shape is chosen to be slab-like, but experiments do not rule out cylinders or connected spheres. Also, it cannot be necessarily expected that the side chains simply pack more densely with decreasing equivalent weight; equally well (and more likely), the pore surface area will be larger as in the simulations presented here, leading to pores of smaller width. Such effects can rigorously be included only in realistic water/Nafion two-phase simulations, where the system size must be large enough to allow for pore fluctuations and for the simultaneous existence of several pores.

Acknowledgements

This work has been performed as a part of a project "Membranes and Membrane Electrode Assemblies for Direct Methanol Fuel Cells" supported by the German government under BMWi Grant 0327086. I wish to thank the John von Neumann Institut für Computing (NIC) at the Forschungszentrum Jülich for generous amounts of computer time and acknowledge helpful discussions with P. Commer, C. Hartnig and A. A. Kornyshev.

References

[1] Gottesfeld, S. and Zawodzinski, T.A. (1997) "Advances in electrochemical science and engineering", In: Alkire, R.C., Gerischer, H., Kolb, D.M. and Tobias, C.W., eds, *Polymer Electrolyte Fuel Cells* (Wiley-VCH, Weinheim) Vol. 5, pp 195–301.
[2] Büchi, F.N., Scherer, G.G., Wokaun, A., eds, (2001) *1st European PEFC Forum, 2–6 July, Lucerne, Switzerland* (European Fuel Cell Forum, Oberrohrdorf, Switzerland).
[3] Pineri, M. (1987) In: Eisenberg, A., ed, *Structure and Properties of Ionomers* (Reidel Publishing Co., Dordrecht, Holland).
[4] Eisenberg, A., ed, (1982) *Perfluorinated Ionomer Membranes* ACS Symposium Series. Topical Workshop Lake Buena Vista, (American Chemical Society, Washington, DC) Vol. 180.

[5] Heitner, W.C. (1996) "Recent advances in perfluorinated ionomer membranes: structure, properties and applications", *J. Membr. Sci.* **120**, 1.

[6] Cappadonia, M., Kornyshev, A.A., Krause, S., Kuznetsov, A.M. and Stimming, U. (1994) "Low-temperature proton transport in clathrates", *J. Chem. Phys.* **101**, 7672.

[7] Cappadonia, M., Erning, J.W., Niaki, S.M.S. and Stimming, U. (1995) "Conductance of Nafion 117 membranes as a function of temperature and water content", *Solid State Ionics* **77**, 65.

[8] Eikerling, M., Kornyshev, A.A. and Stimming, U. (1997) "Electrophysical properties of polymer electrolyte membranes: a random network model", *J. Phys. Chem. B* **101**, 10807.

[9] Eikerling, M., Kornyshev, A.A., Kuznetsov, A.M., Ulstrup, J. and Walbran, S. (2001) "Mechanisms of proton conductance in polymer electrolyte membranes", *J. Phys. Chem. B* **105**, 3646.

[10] Eikerling, M. and Kornyshev, A.A. (2001) "Proton transfer in a single pore of a polymer electrolyte membrane", *J. Electroanal. Chem.* **502**, 1.

[11] von Grotthus, C.J.D. (1806) "Mémoire sur la décomposition de l'eau et des corps qu'elle tien en dissolution à l'aide de l'électricité galvanique", *Ann. Chim.* **LVIII**, 54.

[12] Marx, D., Tuckerman, M.E., Hutter, J. and Parrinello, M. (1999) "The nature of the hydrated excess proton in water", *Nature* **397**, 601.

[13] Vishynakov, A. and Neimark, A.V. (2001) "Molecular dynamics simulation of microstructure and molecular mobilities in swollen Nafion membranes", *J. Phys. Chem. B* **105**, 9586.

[14] Vishnyakov, A. and Neimark, A.V. (2000) "Molecular simulation study of Nafion membrane solvation in water and methanol", *J. Phys. Chem. B* **104**, 4471.

[15] Vishynakov, A. and Neimark, A.V. (2001) "Molecular dynamics simulation of Nafion oligomer solvation in equimolar methanol–water mixture", *J. Phys. Chem. B* **105**, 7830.

[16] Ennari, J., Elomaa, M. and Sundholm, F. (1999) "Modelling a polyelectrolyte system in water to estimate the ion conductivity", *Polymer* **40**, 5035.

[17] Paddison, S.J., Pratt, L.R., Zawodzinski, T. and Reagor, D.W. (1998) "Molecular modeling of trifluoromethanesulfonic acid for solvation theory", *Fluid Phase Equil.* **150–151**, 235.

[18] Paddison, S.J. and Zawodzinski, T. Jr, (1998) "Molecular modeling of the pendant chain in Nafion", *Solid State Ionics* **113–115**, 333.

[19] Paddison, S.J., Pratt, L.R. and Zawodzinski, T.A. Jr. (2001) "Variation of the dissociation constant of triflic acid with hydration", *J. Phys. Chem. A* **105**, 6266.

[20] Eikerling, M., Paddison, S.J. and Zawodzinski, T.A. Jr. (2002) "Molecular orbital calculations of proton dissociation and hydration of various acidic moieties for fuel cell polymers", *J. New Mat. Electr. Sys.* **5**, 15.

[21] Fornili, S.L., Migliore, M. and Palazzo, M.A. (1986) "Hydration of the hydronium ion. *Ab initio* calculations and Monte Carlo simulations", *Chem. Phys. Lett.* **125**, 419.

[22] Chialvo, A.A., Cummings, P.T. and Simonson, J.M. (2000) "H_3O^+/Cl^- ion-pair formation in high-temperature aqueous solutions", *J. Chem. Phys.* **113**, 8093.

[23] Zahn, D. and Brickmann, J. (1999) "Quantum-classical simulation of proton migration in water", *Isr. J. Chem.* **39**, 469.

[24] Zahn, D. and Brickmann, J. (2000) "A comparative study of proton migration in water and deuteron transport in heavy water by means of mixed quantum/classical molecular dyanmics simulation", *Chem. Phys. Lett.* **331**, 224.

[25] Tuckerman, M., Laasonen, K., Sprik, M. and Parrinello, M. (1995) "*Ab initio* molecular dynamics simulation of the solvation and transport of H_3O^+ and OH^- ions in water", *J. Phys. Chem.* **99**, 5749.

[26] Tuckerman, M., Laasonen, K., Sprik, M. and Parrinello, M. (1995) "*Ab initio* molecular dynamics simulation of the solvation and transport of hydronium and hydroxyl ions in water", *J. Chem. Phys.* **103**, 150.

[27] Tuckerman, M., Marx, D., Klein, M. and Parrinello, M. (1997) "On the quantum nature of the shared proton in hydrogen bonds", *Science* **275**, 817.

[28] Laasonen, K.E. and Klein, M.L. (1997) "*Ab initio* study of aqueous hydrochloric acid", *J. Phys. Chem. A* **101**, 98.

[29] Marx, D., Tuckerman, M.E. and Parrinello, M. (2000) "Solvated excess protons in water: quantum effects on the hydration structure", *J. Phys.: Cond. Matter* **12**, A153.

[30] Geissler, P.L., Dellago, C., Chandler, D., Hutter, J. and Parrinello, M. (2001) "Autoionization in liquid water", *Science* **291**, 2121.

[31] Lobaugh, J. and Voth, G.A. (1996) "The quantum dynamics of an excess proton in water", *J. Chem. Phys.* **104**, 2056.

[32] Vuilleumier, R. and Borgis, D. (1998) "Quantum dynamics of an excess proton in water using and extended empirical valence-bond Hamiltonian", *J. Phys. Chem. B* **102**, 4261.

[33] Vuilleumier, R. and Borgis, D. (1998) "An extended empirical valence bond model for describing proton transfer in $H^+(H_2O)_n$ clusters and liquid water", *Chem. Phys. Lett.* **284**, 71.

[34] Schmitt, U.W. and Voth, G.A. (1998) "Multistate empirical valence bond model for proton transport in water", *J. Phys. Chem. B* **102**, 5547.

[35] Vuilleumier, R. and Borgis, D. (1999) "Transport and spectroscopy of the hydrated proton: a molecular dynamics study", *J. Chem. Phys.* **111**, 4251.

[36] Schmitt, U.W. and Voth, G.A. (1999) "The computer simulation of proton transport in water", *J. Chem. Phys.* **111**, 9361.

[37] Cuma, M., Schmitt, U.W. and Voth, G.A. (2000) "A multi-state empirical valence bond model for acid base chemistry in aqueous solution", *Chem. Phys.* **258**, 187.

[38] Schmitt, U.W. and Voth, G.A. (2000) "The isotope substitution effect on the hydrated proton", *Chem. Phys. Lett.* **329**, 36.

[39] Walbran, S. and Kornyshev, A.A. (2001) "Proton transport in polarizable water", *J. Chem. Phys.* **114**, 10039.

[40] Spohr, E., Commer, P. and Kornyshev, A.A. (2002) "Enhancing proton mobility in polymer electrolyte membranes: lessons from molecular dynamics simulations", *J. Phys. Chem. B* **106**, 10560.

[41] Mayo, S.L., Olafson, B.D. and Goddard, III, W.A. (1990) "Dreiding: a generic force field for molecular simulations", *J. Phys. Chem.* **94**, 8897.

[42] Berendsen, H.J.C., Postma, J.P.M., van Gunsteren, W.F., DiNola, A. and Haak, J.R. (1984) "Molecular dynamics with coupling to an external bath", *J. Chem. Phys.* **81**, 3684.

[43] Kornyshev, A.A., Kuznetsov, A.M., Spohr, E. and Ulstrup, J. (2003), *J. Phys. Chem. B*, in press.

[44] Gierke, T.D., Munn, G.E. and Wilson, F.C. (1981) "The morphology in Nafion perfluorinated membrane products, as determined by wide-angle and small-angle x-ray studies", *J. Polymer Sci. Part B-Polymer Phys.* **19**, 1687.

[45] Dreyfus, B., Gebel, G., Aldebert, P., Pineri, M., Escoubes, M. and Thomas, M. (1990) "Distribution of the micelles in hydrated perfluorinated ionomer membranes from SANS experiments", *J. Phys. (France)* **51**, 1341.

[46] Gebel, G. and Lambard, J. (1997) "Small-angle scattering study of water-swollen perfluorinated inomer membranes", *Macromolecules* **30**, 7914.

[47] Rollet, A.-L., Diat, O. and Gebel, G. (2002) "A new insight into Nafion structure", *J. Phys. Chem. B* **106**, 3033.

[48] Gordeliy V.I., Technical report, Dept of Molecular and Biological Physics, Moscow Institute for Physics and Technology (2001).

[49] Gordeliy V.I., Islamov A., Kornyshev A.A., Mergel J., to be published.

[50] Commer P., Kornyshev A.A., Spohr E., in preparation.